**Preprint Title** Soybean-derived blue photoluminescent carbon dots

**Authors** Shanshan Wang, Wei Sun, Dong-sheng Yang and Fuqian Yang

**Publication Date** 05 Nov 2019

**Article Type** Full Research Paper

**Supporting Information File 1** soybean supporting information.docx; 4.3 MB

**ORCID® iDs** Dong-sheng Yang - https://orcid.org/0000-0001-9842-4343; Fuqian Yang - https://orcid.org/0000-0001-6277-3082

# Soybean-derived blue photoluminescent carbon dots

*Shanshan Wang* [a,b], *Wei Sun* [c], *Dong-sheng Yang* [a] * *and Fuqian Yang* [b]*

[a] Department of Chemistry, University of Kentucky, Lexington, KY 40506, United States

[b] Materials Program, Department of Chemical and Materials Engineering

University of Kentucky, Lexington, KY 40506, United States

[c] College of Chemistry, Chemical Engineering and Environmental Engineering,

Liaoning Shihua University, Fushun, Liaoning, 113001, China

**Abstract**

Biomass-derived carbon dots (CDs) are biocompatible and have the potential in a variety of applications, including bio-imaging and bio-sensing. In this work, we use ground soybean residuals to synthesize carbon nanoparticles by hydrothermal carbonization (HTC), annealing at high temperatures, and laser ablation (LA) in a $NH_4OH$ solution. The carbon nanoparticles synthesized with the HTC process (HTC-CDs) exhibit photoluminescent characteristics with strong blue emission. The annealing of the HTC-CDs at temperatures in a range of 250 to 850 $^{o}$ C causes the loss of the photoluminescent characteristics without any significant changes in the microstructures (amorphous structure) of carbon particles. The LA processing of the annealed HTC-CDs introduces nitrogen-contained surface-functional groups and leads to the recovery of the photoluminescent features that are different from those of the HTC-CDs and dependent on the fraction of nitrogen in the surface-functional groups. The photoluminescence of both the HTC-CDs and LA-CDs is largely due to the presence of N-contained surface-functional groups. The quantum yield of the LA-CDs is more stable than that of the HTC-CDs under continuous UV excitation and does not exhibit significant reduction over 150 min excitation. The methods used in this work provide a simple and green strategy to introduce surface-functional groups to carbon nanoparticles from biomass and biowaste and to produce stable photoluminescent CDs with excellent water-wettability.

**Keywords:** biomass; carbon dots; hydrothermal process; laser ablation; photoluminescence.

Corresponding Authors: Email: fyang2@uky.edu (FQY), Dong-Sheng.Yang@uky.edu (DSY)

## 1. Introduction

Carbon dots (CDs), which are carbon-based quantum dots [1], have attracted great interest due to their unique properties, such as less-toxicity, eco-friendly environment [2,3], high water solubility [4], high chemical stability [5], high photostability [6], tunable excitation and emission wavelengths [7], and low cost [8]. CDs have been considered as a group of important nanomaterials with potential applications in nanotechnology [9], electrocatalysis [10], metal-ion detection [2], thermal sensing [11], drug delivery [12], and biosensing and bioimaging [1].

Several methods are available for synthesizing CDs, including oxidation and reduction [13-15], laser ablation [15], microwave irradiation [9], pyrolysis [16], and hydrothermal treatment [17]. Some of these methods are tedious and time consuming and use strong acids and/or surface treatment to improve their water solubility and luminescence property. Hydrothermal carbonization (HTC), which can be considered as "green", has been used to produce photoluminescent CDs from biomass, including glucose, sucrose, citric acid [18], chitosan [19], orange juice [20], grass [21] and soy milk [10]. For example, Sahu et al. [20] synthesized photoluminescent CDs of 1.5-4.5 nm in sizes from orange juice at 120 $^{o}$C. Liu et al. [21] produced photoluminescent polymer nanodots of 3-5 nm in diameter by using grass as a precursor at 180 $^{o}$C, and Zhu et al. [10] synthesized bifunctional blue-emission carbon nanodots with diameters of 13-40 nm from soy milk also at 180 $^{o}$C.

Laser ablation in liquid (LAL) has been used to produce nanomaterials with special morphologies, microstructures, and phases and with various functionalized nanostructures [22–24]. For example, carbon-based nanoparticles with fewer side-products have been synthesized from glassy carbon [15], graphite [25], polymethyl methacrylate (PMMA) [26], and a graphite-cement mixture [6] via LAL in various liquids.

In general, there are two major mechanisms contributing to the photoluminescence (PL) of CDs: one is the size-dependent bandgap, and the other is the surface states consisting of functional groups [27]. Other factors, such as conjugated π-domains, molecular states, and crosslink-enhanced emission, need to be taken into account in the understanding of the PL emission of CDs [28]. Also, the PL behavior of CDs varies with pH and temperature [17]. Wang et al. [17] studied the fluorescence of the CDs made from glucose with glutathione in a temperature

range of 15 to 90 ° C and observed the change of the fluorescent color from dark blue to light blue and the quenching of the fluorescence at high temperatures. They attributed the fluorescent quenching to the aggregation of CDs, which increased particle sizes from 2.6 ± 0.2 to 4.4 ± 0.2 nm. However, studies are hard to find in the literature for comparing the PL behavior of CDs made from the same biomass precursor with different synthetic or processing methods; such studies would provide the insight into the CD formation and PL mechanisms.

Considering the potential applications of CDs in bioimaging and biosensing, we synthesize bio-compatible CDs from soybean residuals using two strategies. The first strategy uses one-step HTC process to produce CDs directly from the soybean residuals, and the second one uses multiple steps to produce CDs from the same soybean precursors, which involves the HTC treatment, high-temperature annealing, and LAL processing, sequentially. The purpose of the LAL processing is to introduce N-contained functional groups onto the surface of carbon nanoparticles and to recover the PL of carbon nanoparticles/CDs that was quenched by the high-temperature annealing. Both methods can be categorized as the group of top-down methods in contrast to the bottom-up methods. The PL characteristics of the CDs produced by both methods are analyzed, and the PL mechanisms the CDs are discussed. The strategies developed in this work offer simple and effective means for producing bio-compatible CDs from biomass and biowaste and manipulating their PL characteristics.

## 2. Experimental details

### 2.1 Hydrothermal carbonization

The materials used to produce CDs were a ground soybean residual and sulfuric acid. The ground soybean residual was collected as waste after the grounding of soybean in water. A suspension consisting of ~ 40 g of the ground soybean residual and ~ 5 mL of 1 wt.% $H_2SO_4$ aqueous solution was prepared and stirred ultrasonically. The suspension was transferred into a Teflon-lined autoclave, which was then placed in an oven for the HTC processing at 200 °C for 20 h. After the temperature of the Teflon-lined autoclave was cooled to room temperature in air, filtration with 10 μm pore-size filter papers was performed to separate the HTC-produced mixture. The filtrate was further filtrated with 450 nm pore size filter papers. The material collected after the filtration was dried at 60 °C in a vacuum oven for 24 h, and the final product

was named as HTC-CDs.

## 2.2 High-temperature annealing

The high-temperature annealing was performed in a horizontal tube furnace under the flow of argon gas. A quartz boat loaded with HTC-CDs was placed in the tube around the center of the hot zone. The tube furnace was first flushed at room temperature with argon gas at a flow rate of 300 SCCM (standard cubic centimeters per minute) for 30 min, then heated up to a pre-set annealing temperature, 850 °C, at a ramping rate of 20 °C/s under the flow of argon gas at a flow rate of 50 SCCM, and finally maintained at 850 °C for 2 h to anneal the HTC-CDs. After the annealing, the temperature of the furnace/system was reduced to room temperature in air. The black carbon powders, which formed in the quartz boat, were collected and named as annealed-CDs.

## 2.3 Laser ablation in $NH_4OH$ solution

Figure 1 illustrates the process for the synthesis of CDs from the ground soybean residual and the setup of laser ablation of annealed-CDs in $NH_4OH$ aqueous solution. Using a prism and an optical lens shown in Fig. 1, the beam size of laser was adjusted to ~2 mm. The laser wavelength was 532 nm, the pulse frequency was 50 Hz, and the dwell was 1-2 ns.

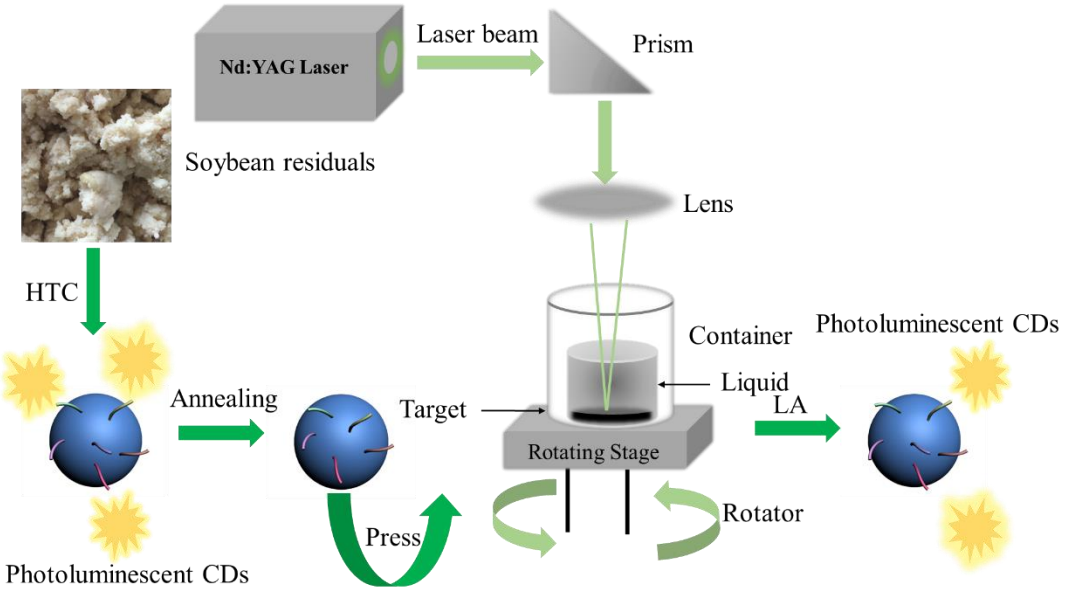


**Figure 1.** Schematic of the setup for laser ablation in liquid.

A mixture consisting of ~ 0.06 g annealed-CDs and 0.012 g Teflon powder was heated to 110 °C and maintained at 110 °C for 1 h. Mechanical press of the heated mixture at 6000 psi

for 5 min led to the formation of a circular pellet of ~1.27 cm in diameter and ~1 mm in thickness. The circular pellet was transferred to a self-made vial container with a quartz window for the laser ablation, and ~3 mL $NH_4OH$ aqueous solution was added to the vial container to submerse the pellet to a depth of 2 cm. A quartz window lid was used to minimize the loss of the $NH_4OH$ solution during the laser ablation. The vial container was placed on the top of the rotation stage. The rotation of the glass vial ensured each laser pulse impinged on a fresh surface of the pellet.

The LAL processing of the annealed-CDs in the $NH_4OH$ solution was performed with a pulse energy of 100 mJ for 1 h. After the LAL processing, the liquid remained in the vial container was collected and filtered with a 0.45 μm syringe prior to analysis. After all solvents were evaporated, 4 mL DI (deionized) water was added to the glass vial to form a suspension, which was sonicated for 1 h at room temperature. $NH_4OH$ solutions of concentrations of 5%, 15%, 20% and 30% in volume were used in the LAL processing. The obtained LA samples were named as LA-CDs-x% with x representing the concentration of the $NH_4OH$ solution.

2.4 Materials characterization

The morphologies and microstructures of the prepared carbon nanoparticles were characterized on a transmission electron microscope (TEM) (JEOL 2010F). ImageJ software was used to analyze the TEM images and determine the distribution of particle sizes for the calculation of average particle size. The XPS (X-ray photoelectron spectroscopy) analysis of the prepared carbon nanoparticles was conducted on a Thermo Scientific K-Alpha X-ray photoelectron spectrometer to determine the chemical states of elements in the prepared carbon nanoparticles.

The PL characteristics of the prepared carbon nanoparticles were characterized on a fluorometer (HORIBA, Fluoromax-3) equipped with a xenon lamp of 120 W as the light source. The absolute QY (quantum yield) was measured on a second fluorometer (Horiba Fluoromax-4) equipped with an integrating sphere. A quartz cubic cell of 1 cm in the light path, which was filled with a suspension consisting of the prepared carbon nanoparticles, was used in UV-Vis absorption measurement, which was performed on an UV-Visible spectrophotometer (Thermal Scientific Evolution 201). The FT-IR (Fourier-transform infrared spectroscopy) analysis of the

prepared carbon nanoparticles was conducted on a Fourier transform infrared instrument (Nicolet iS50) in the wavenumber range of 400 to 4000 $cm^{-1}$ at a resolution of 4 $cm^{-1}$.

## 3. Results

Figure 2 shows TEM images of the soybean-derived nanoparticles and the corresponding size distribution. All the nanoparticles are in a polygonal shape (Fig. 2a-c), suggesting that the annealing at high temperatures and the laser ablation did not cause any significant changes to the morphologies of the nanoparticles. The SAED (selected area electron diffraction) patterns embedded in the figures reveal that all the nanoparticles are amorphous. The EDS and XPS analyses of the HTC-CDs shown in Fig. S1 and Table. S1 in Supplementary Information confirm that the main component of the HTC-CDs is carbon. The annealing at the temperature of 850 °C did not cause the conversion of amorphous carbon nanoparticles to nanocrystals, and the LAL processing of the annealed-CDs also produced amorphous carbon nanoparticles.

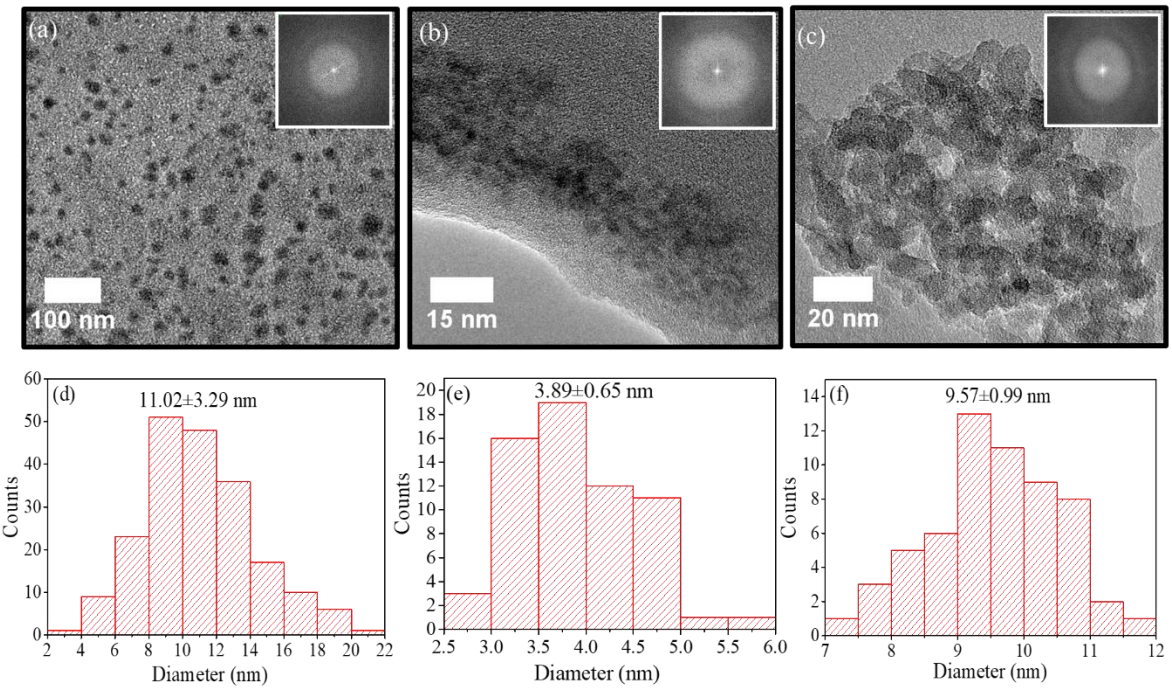


**Figure 2.** TEM images of soybean-derived nanoparticles: (a) HTC-CDs, (b) annealed-CDs (annealing temperature: 850 °C), and (c) LA-CDs-10%; the size distribution of soybean-derived nanoparticles: (d) HTC-CDs, (e) annealed-CDs, and (f) LA-CDs-10%.

The size distribution of the soybean-derived nanoparticles is depicted in Fig. 2d-f, which

was determined from the TEM images via the software of ImageJ. Slight differences are observed in the shapes of the size distribution among the HTC-CDs, annealed-CDs and LA-CDs-10%. All the histograms are approximately in a λ-shape. The histogram of the HTC-CDs has a long tail in the distribution; the histogram of the annealed-CDs is close to Gaussian distribution; and the histogram of the LA-CDs-10% has a long front in the distribution. The mechanism for the differences in the shape of the size distribution is unclear and might be due to the effects of high-temperature annealing and laser ablation on the motion of atoms. From the size distribution, we obtain the average particle sizes of the soybean-derived nanoparticles as 11.02±3.29, 3.89±0.65 and 9.57±0.99 nm for the HTC-CDs, annealed-CDs and LA-CDs-10%, respectively. The observed average particle sizes are different from the amorphous CDs of 2.6 ± 0.2 nm made from glucose with glutathione in a temperature range of 15 to 90 ° C by Wang et al. [17].

Figure 3a-c shows the PL spectra of the soybean-derived CDs. The HTC-CDs exhibited strong emission under the irradiation of UV and visible light with wavelength in a range of 250 nm to 480 nm (Figs. 3a), indicating the broad PL characteristics of the HTC-CDs. The broad multicolor emission can be attributed to the heterogeneity of CDs due to structural variety [1], including surface-functional groups and domain structures, and to the broad absorption ranging from UV to visible light [29]. There are three strong emission peaks at 423, 440, and 452 nm for the HTC-CDs, which are excited by the UV-vis light with the wavelengths of 330, 360 and 390 nm.

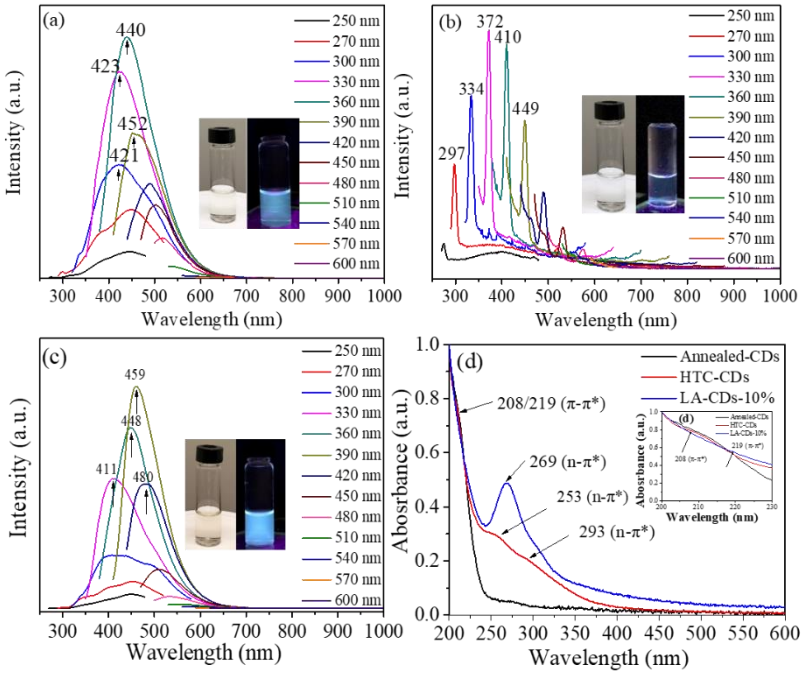


**Figure 3.** Photoluminescence spectra of: (a) HTC-CDs, (b) annealed-CDs, and (c) LA-CDs-10%; (d) UV-Vis absorbance spectra of different soybean-derived CDs.

Sharp peaks presented in the PL spectrum for the annealed-CDs (Fig. 3b), which are significantly different from those for the HTC-CDs and LA-CDs-10%, are due to the Raman scattering of the water [30]. The annealed-CDs show no PL characteristics under the irradiation of the UV-Vis light.

In contrast to the annealed-CDs, the LA-CDs-10%, which are produced by the laser ablation of the annealed-CDs, exhibited strong emission under the irradiation of UV-Vis light with wavelength in the range of 250 to 480 nm. For example, the wavelength and FWHM (full width at half maximum) of the maximum emission peak are 459 nm and 91 nm, respectively, under the irradiation of the light of 390 nm. Comparing the PL spectrum of the LA-CDs-10% with that of the HTC-CDs, we note a blue shift from 423 nm emission of the HTC-CDs to 411 nm emission of the LA-CDs-10% with 330 nm excitation.

The difference in the PL characteristics can also be observed from the insets in Fig. 3a-c. The color of the aqueous solutions of both the HTC-CDs and LA-CDs-10% is light-yellow under white light and blue under the UV light of 365 nm. However, there is no difference in color between the aqueous suspension of the annealed-CDs under white light and 365 nm

excitation.

The UV−Vis spectra of the HTC-CDs, annealed-CDs and LA-CDs-10% are depicted in Fig. 3d. There are three peaks at 208, 253 and 293 nm for the HTC-CDs. The peak at 208 nm is from the π-π* transition of the conjugated C=C band on the backbone of carbon [31], and the peaks of the broad absorbance at 253 and 293 nm are from the n-π* transition of the carbonyl and other oxygen or nitrogen-containing groups [32]. There is no visible peak for the annealed-CDs, which exhibited continuous-weak absorbance in the wavelength range of 200 to 250 nm. Such a result suggests that the annealed-CDs are of metallic characteristics with zero bandgap [33].

For the LA-CDs-10%, there are a small shift of 219 nm for the peak corresponding to the π-π* transition and an increase in the intensity for the peak corresponding to the n-π* transition. The strong and broad absorption band is over the range of 240 to 350 nm with a peak at 269 nm, which can be ascribed to the complex transitions on the surface from the n-π* transitions in the groups of C=O and/or C=OOH [1, 10, 36]. The long tail extending to the visible light can be attributed to the amino groups on the surface of the CDs [35]. Note that the LA-CDs-x% produced from the LAL processing of the annealed-CDs in the $NH_4OH$ solutions of different concentrations also exhibited strong absorption near 270 nm, which is attributed to n-π* transition, as shown in Figure S4f in Supplementary Information. The significant differences in the wavelength and intensity of the n-π* transition between the HTC-CDs and the LA-CDs-10% suggest that the functional groups and the fractions of the functional groups on the HTC-CDs are significantly different from those on the LA-CDs-10%.

In summary, all three CDs exhibit strong π-π* absorption; the HTC-and LAL-CDs possess strong n-π* absorption, while there is no significant n-π* absorption from the annealed-CDs. Coupling the UV-Vis absorption spectra with the PL spectra, we suggest that the observed PL originates from excited states produced by the n-π* excitation or from functionalized surface states.

The TCSPC (Time-Correlated Single Photon Counting) lifetime measurement was performed under 393 nm irradiation nm, and the emission was recorded at 440, 452, and 459 nm since the HTC-CDs exhibited the strongest emission at 440 nm, the LA-CDs-10% exhibited

the strongest emission at 459 nm, and both exhibited moderate emission at 452 nm. The instrument response function was determined from the analysis of the scattering of a Ludox solution at the 393 nm excitation.

Figure 4a-b shows the PL decay curves of the HTC-CDs at the 440 nm emission and the LA-CDs-10% at the 459 nm emission. According to Fig. 4a-b, we expect similar behavior for the intensity of the emission light. Assuming that the PL decay curves can be described by a triple-exponential function [33]

$$N(t) = A + \sum_{i=1}^{3} B_i e^{-t/\tau_i} \quad (1)$$

where $N(t)$ is the number of the photons emitted at time $t$, $A$ represents the baseline/noise level, $B_i$ ($i$=1, 2, 3) are proportional constants for the corresponding decay functions, and $\tau_i$ are the lifetimes. Using Eq. (1) to fit the PL decay curves in Fig. 4a-b, we obtain the lifetimes of $\tau_i$ and the constants of $B_i$. The fitting curves are included in the corresponding figures. It is evident that Eq. (1) can well describe the 440 and 459 nm PL-decay behavior of the HTC-CDs and the LA-CDs-10%, respectively. .

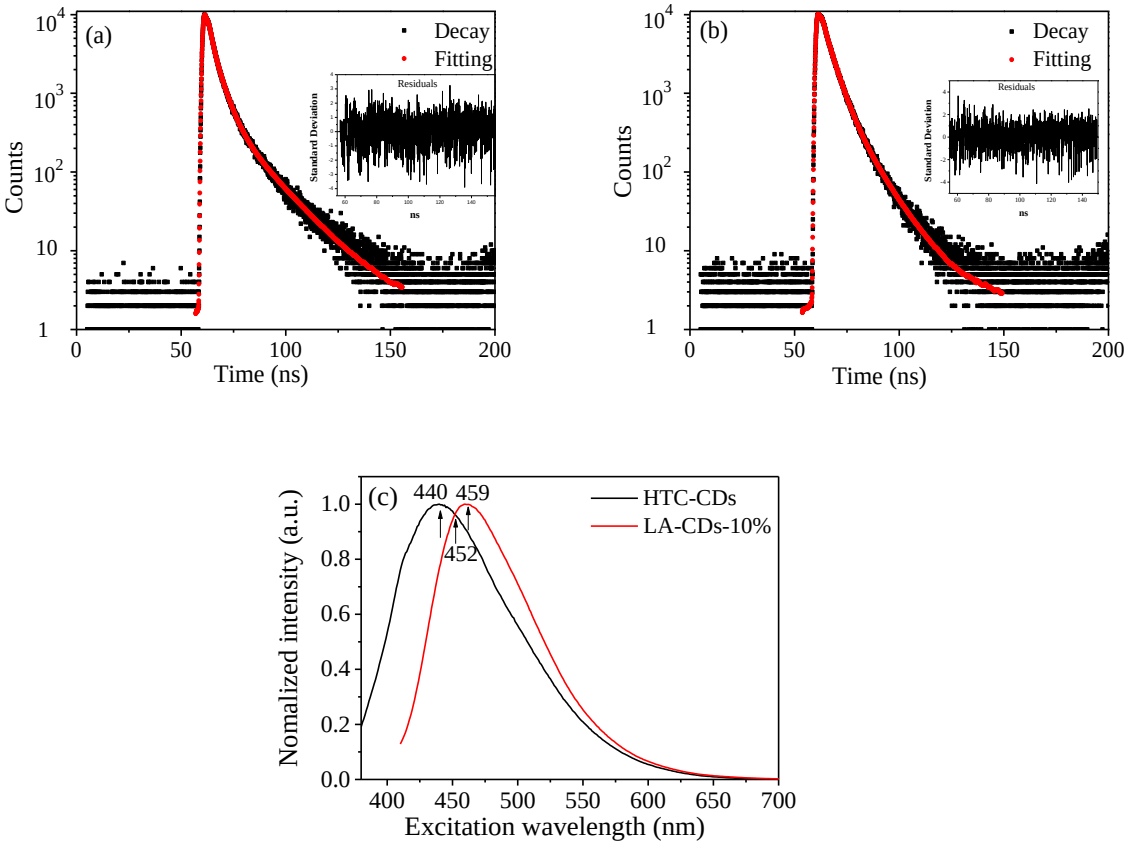

**Figure 4**. TCSPC lifetime curves under the 393 nm excitation: (a) HTC-CDs for the 440 nm emission, and (b) LA-CD-10% for the 459 nm emission (The red lines represent the fitting curves, and the insets depict the residues for the fittings.); (c) overlaid emission spectra of the HTC-CDs and LA-CDs-10% under the 393 nm excitation.

Table 1 lists the lifetimes and the corresponding contributions obtained from the curve fitting. It is evident that the PL decays of both the HTC-CDs and LA-CDs-10% consist of three rate processes with the fastest one, $\tau_1$, attributed to the intrinsic state of the CDs, and two slower processes, $\tau_2$ and $\tau_3$, attributed to the decays of the extrinsic states associated with the surface-functional groups on CDs [33,36]. According to Table 1, the slower process, $\tau_2$, contributes more than 50% to the PL decay.

**Table 1.** Lifetimes ($\tau_1$, $\tau_2$ and $\tau_3$) of the emission lights ($\lambda_{em}$) and the relative ratios ($R_i=B_i/(B_1+B_2+B_3)$) (%) for the HTC-CDs and LA-CDs-10% under the 393 nm excitation.

| $\lambda_{ex}$=393 nm | $\lambda_{em}$ (nm) | $\tau_1$ (ns) | $R_1$ (%) | $\tau_2$ (ns) | $R_2$ (%) | $\tau_3$ (ns) | $R_3$ (%) |
|---|---|---|---|---|---|---|---|
| HTC-CDs | 440 | 1.21(3) | 28.6 | 4.24(4) | 52.8 | 15.0(1) | 18.6 |
| | 452 | 1.05(3) | 24.4 | 4.23(4) | 55.0 | 13.57(8) | 20.6 |
| | 459 | 1.14(4) | 24.6 | 4.41(3) | 55.1 | 14.01(7) | 20.3 |
| LA-CDs-10% | 440 | 0.74(4) | 14.0 | 4.13(3) | 65.4 | 10.58(7) | 20.6 |
| | 452 | 0.76(4) | 12.3 | 4.18(4) | 64.9 | 10.31(7) | 22.8 |
| | 459 | 1.01(6) | 12.2 | 4.38(3) | 66.8 | 10.82(7) | 21.0 |

Figure 5 shows the temporal variation of the QY of the HTC-CDs under 360 nm continuous excitation and the LA-CDs-x% with 390 nm continuous excitation. Each measurement took about 30 min. The HTC-CDs displayed the largest QY initially, and the QY decreased gradually with the increase of the excitation time to 35.2% of the initial QY after the continuous excitation of 150 min. Such behavior might be attributed to the photobleaching associated with photo-induced changes in the structure of the functional groups on the surface of CDs [37].

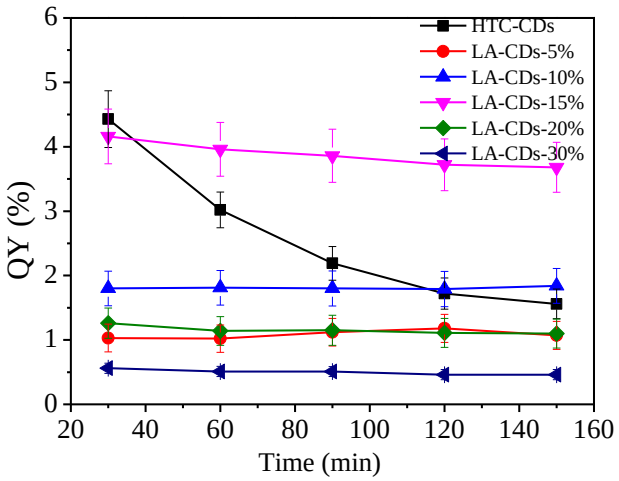


**Figure 5.** Temporal evolution of quantum yield for the HTC-CDs under the 360 nm excitation and the LA-CDs-x% under the 390 nm excitation (Each measurement took about 30 min. The fluorescence intensity was calculated by integrating over the wavelength range of 340-700 nm for the HTC-CDs and 370-760 nm for the LA-CDs-x%.)

In contrast to the temporal variation of the QY of the HTC-CDs, the QY of the LA-CDs-x% is much stable under 390 nm irradiation and did not exhibit significant reduction over the 150 min excitation. For the LA-CDs-x% with x=5, 10, 20, and 30, the QYs remained approximately unchanged. The LA-CDs-15% displayed the largest QY among the LA-CDs,which is compatible with the largest QY of the HTC-CDs and shows only 11.5% decrease after 150 min irradiation. The mecahnisms for such behavior are unclear. It might be due to the relatively uniform sizes of the CDs and/or the strong bonding between the functional groups and the CDs after the LAL processing.

## 4. Discussion

Table 2 summarizes the PL characteristics of the HTC-CDs, annealed-CDs and LA-CDs-10% under 330, 360 and 390 nm excitation, respectively. All the annealed-CDs in the annealing temperature range of 250 to 850 °C did not exhibit any PL characteristics by the excitation of all three wavelengths. It is known that two controlling mechanisms determine the PL characteristics: one is the domain size of CDs, and the other is the functional groups over the surface of CDs. With the annealing temperature in the range of 250 to 850 °C, there is no significant change in the microstructure (amorphous structure) of carbon nanoparticles, suggesting that annealing did not likely cause any significant changes to the domain sizes in

the HTC-CDs. Note that annealing did cause the change in the particle size irregularly. Thus, it is the functional groups on the surface of CDs that play the key role in the light emission of the soybean-derived CDs under the excitation of UV light.

**Table 2.** PL characteristics of the synthesized CDs

| Excitation wavelength (nm) | HTC-CDs | | Annealed-CDs | | LA-CDs-10% | |
|---|---|---|---|---|---|---|
| | Emission peak (nm) | FWHM (nm) | Emission peak (nm) | FWHM (nm) | Emission peak (nm) | FWHM (nm) |
| 330 | 423 ± 3 | 129 | NA | | 411 ± 3 | 122 |
| 360 | 440 ± 1 | 109 | NA | | 448 ± 2 | 203 |
| 390 | 452 ± 3 | 109 | NA | | 459 ± 2 | 91 |
| QY (%) | 4.46 | | NA | | 1.81 | |

* FWHM=Full width at half maximum

Comparing the PL characteristics of the HTC-CDs with those of the LA-CDs-10%, we note the differences in the emission wavelength and the FWHM. Such differences reveal that the functional groups on the surface of the HTC-CDs are likely different from those on the surface of the LA-CDs-10%. Annealing the HTC-CDs damaged/destroyed the surface structures/ function groups, resulting in the complete loss of the PL characteristics. The LAL processing of the annealed-CDs in $NH_4OH$ aqueous solution introduced "new" functional groups to the surface of the CDs, leading to the "re-birth" of the PL characteristics. It is interesting to note that there are large fluctuations in the FWHM for the LA-CDs-10%, which is likely attributed to the fluctuations of the bandgap associated with the functional groups and the disorder of crystallinity introduced by the LAL processing.

According to Yu et al. [38], the emission peak of CDs can be fitted with a two-Gaussian function, assocaiated with the "core" state and "surface" state, as shown schematically in Fig. 6. From Fig. 3, we note that the strongest emssion is at 440 nm for the HTC-CDs and 459 nm for the LA-CDs-10%. From Fig. 6, we note that both peaks indeed can be fitted with a two-Gassian function, respectively. The fitting results reveal that the 440 nm emission peak of the HTC-CDs can be fitted by a two-Gaussian function: one with a high energy band (the "core band") has a peakat 430 nm and a FWHM of 69 nm, and the other with a low high energy band (the "surface" band) has a peak at 478 nm and a FWHM of 118 nm; and the 450 nm emssion

of LA-CDs-10% can be fitted by a two-Gaussian function: the "core" band has a peak at 442 nm and a FWHM of 83 nm, and the "surface" band has a peak at 488 nm and a FWHM of 124 nm.

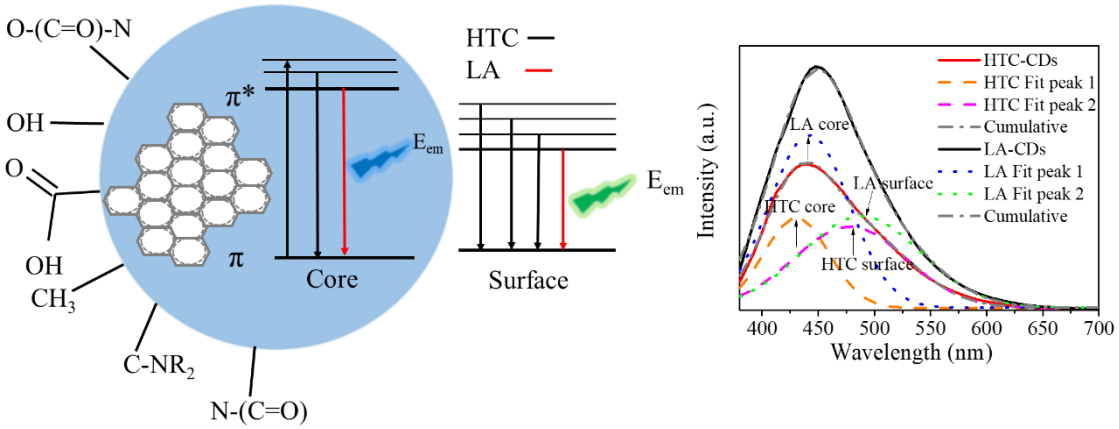


**Figure 6.** Schematic of the bandgaps of CDs under the 360 nm excitation and the deconvolution bands (fitted with Gaussian function)

By integrating both the "core" band and the "surface" band, respectively, we obtain the area ratios of the "surface" band to the "core" band as 1.6 for the HTC-CDs and 1.0 for the LA-CDs-10%. Such a difference in the area ratios (1.6 VS. 1.0) reveals the important role of the "surface" states and surface-functional groups in controlling the PL characteristics of the soybean-derived CDs. The FWHM difference between the strongest emission peaks of the HTC-CDs and LA-CDs-10% is likely attributed to the difference in the "surface" states and surface-functional groups.

Two possibile mechanisms contribute to the loss of the PL characteristics of the annealed-CDs: damaged/destroyed the "surface" states/functional groups and the irreversible change in the energy gap induced by the annealing. It is known that the temperature dependence of the energy gap for the fluoresence of CDs can be expressed as [38]

$$E_g(T) = E_g(0) - 2S < h\omega > (e^{<h\omega>/kT} - 1)^{-1} \qquad (2)$$

where $E_g$ ($T$) is the energy gap at temperature $T$, $S$ is the Huang–Rhys factor representing the coupling strength between exciton and phonon, $<h\omega>$ is the phonon energy, and $k$ is the Boltzmann constant. It is evident that increasing temperature leads to the decrease of the energy gap. CDs become conductive at temperatures larger than the critical temperture and lose the PL charactersistics, as demonstrated by the annealed-CDs due to the irreversible change in the

energy gap at high temperatures.

The PL characteristics of CDs depend on the structure and composition of the CDs, as shown by the FT-IR spectra of the HTC-CDs, annealed-CDs, and LA-CDs-10% in (Figure 7). The FT-IR spectrum of the HTC-CDs is similar to that of the LA-CDs-10%, suggesting the presence of similarly chemical bonding structures. For example, both CDs possess the bands of O-H and N-H stretching vibration at 3344 $cm^{-1}$ and 3366 $cm^{-1}$ [39], respectively. The presence of the O-H and N-H groups makes the CDs hydrophilic and improve the stability and dispersibility of the CDs in aqueous solutions. In addition, there are -N=C=N, N=C=O stretching vibrations represented by the weak bands at 2156 and 2023 $cm^{-1}$ for the HTC-CDs and 2155 and 2063 $cm^{-1}$ for the LA-CDs-10% [41, 42]. The C-H stretching vibrations are at 2931 and 2875 $cm^{-1}$, respectively [7]. The stretching bands of the C=O/C=C bond are around 1706 and 1670 $cm^{-1}$, respectively [42], and the $CH_3$ bending vibrations are at 1375 and 1389 $cm^{-1}$, respectively [33]. The stretching bands of the C–N/C–O bond are at 1096 and 1117 $cm^{-1}$ for the HTC-CDs and the LA-CDs-10%, respectively [35, 41]. Also, there are weak bands in the range of 800 - 600 $cm^{-1}$, corresponding to the bending vibrations of C–O and C–N bonds. Note that the FT-IR spectra of all the LA-CDs-x% reveal the presence of N-contained groups, as shown in Fig. S3f in Supplementary Information, suggesting that the LAL processing of the annealed-CDs introduced N-based functional groups on the surface of CDs.

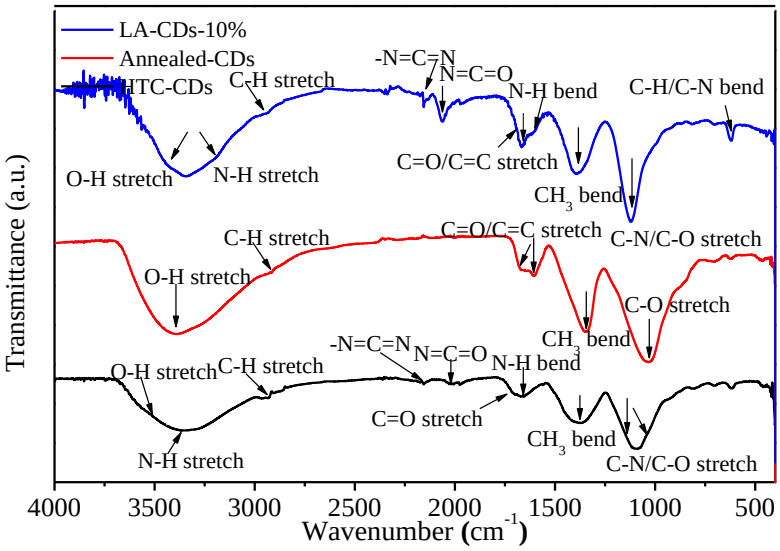


**Figure 7.** FT-IR spectra of soybean-derived carbon nanoparticles.

In contrast to the HTC-CDs and the LA-CDs-x%, the FT-IR spectrum of the Annealed-CDs does not have peaks in the range of 2165–2115 $cm^{-1}$ and 2115–1988 $cm^{-1}$, which are associated with the presence of nitrogen. Such a difference reveals the importance of nitrogen in controlling the PL characteristics of the soybean-derived CDs. It is the N-contained functional groups that determine the PL behavior of both the HTC-CDs and LA-CDs-x%. Note that there is a new peak around 1600 $cm^{-1}$ for the annealed-CDs, which is attributed to aromatic C=C ring band [43,44].

As discussed above, the PL characteristics of the soybean-derived CDs are dependent on the surface-functional groups. XPS analysis was performed to determine the chemical states of elements on the surface of the soybean-derived C-dots. Figure 8 depicts the XPS spectra of the soybean-derived CDs. Table S1 in Supplementary Information lists the chemical compositions on the surface of the soybean-derived CDs, as determined from the XPS analysis. Both the HTC-CDs and LA-CDs-10% contain the elements of C, N and O: 10.3% of N, 6.1% of O and 73.6% of C in the HTC-CDs and 4.4% of N, 44.5% of O and 51.1% of C in the LA-CDs-10%. The ratios of N to C and O to C are 0.14 and 0.08, respectively, for the HTC-CDs and 0.09 and 0.87, respectively, for the LA-CDs-10%. The HTC-CDs is relatively N-rich, and the LA-CDs-10% is O-rich. The differences in the fractions of oxygen and nitrogen likely suggest that the surface-functional groups are different between the two kinds of the CDs leading to the distinct PL responses under the UV-vis irradiation. According to Fig. 8a and Table S1 in Supplementary Information, there is no nitrogen presented in the annealed-CDs, in accord with the FT-IR measurements shown in Fig. 7. This result confirms again the important role of nitrogen in the PL responses of the soybean-derived CDs.

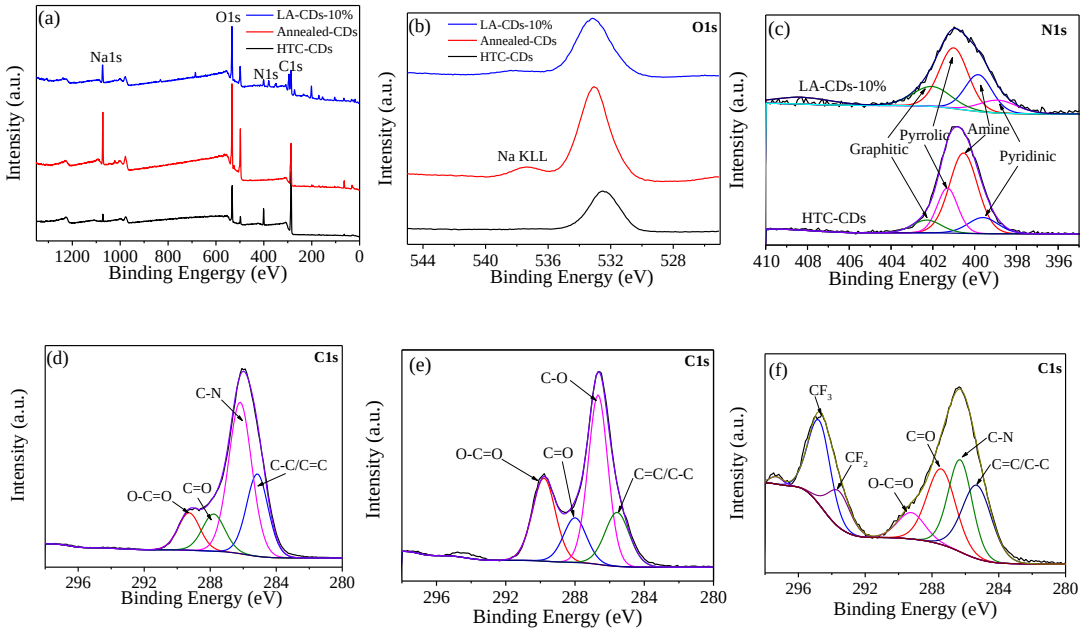


**Figure 8.** (a) XPS survey spectra, (b) deconvoluted high resolution spectra of O1s, (c) deconvoluted high resolution spectra of N1s; deconvoluted high resolution spectra of C1s of (d) HTC-CDs, (e) annealed-CDs, (f) LA-CDs-10%.

Figure 8b-8f shows the deconvoluted high resolution spectra of O1s, N1s and C1s in the soybean-derived CDs. The binding energies of O1s are 532, 533, and 533 eV for the HTC-CDs, annealed-CDs and LA-CDs-10%, respectively, which are deconvoluted to C-O and C=O bands. For the HTC-CDs, the binding energies of N1s determined from the deconvoluted high resolution spectrum of N1s are 398.1, 399.3, 401.5, and 402.1 eV, which are assigned to pyridinic, amine, pyrrolic and graphitic nitrogen, respectively [46, 47]. For the LA-CDs-10%, the binding energies of the corresponding N1s are 398.7, 399.6, 401.0 and 402.1 eV, respectively. Thus, both of the HTC-CDs and the LA-CDs-10% likely possess the same types of the functional groups but with different fractions. The difference in the fractions of the surface-functional groups leads to different PL characteristics.

For the HTC-CDs, the binding energies of C1s are measured to be 285.1, 286.2, 287.8, and 289.3 eV, which are assigned to the C–C/C=C ($sp^3$ and $sp^2$), C–N ($sp^3$), C=O, and O–C=O ($sp^2$), respectively [20, 35, 48, 49]. The binding energies of C1s in the annealed-CDs are 285.6, 286.7, 287.9 and 289.8 eV, corresponding to the C–C/C=C, C-O, C=O and O-C=O groups, while the binding energies of C1s in the LA-CDs-10%, are 294.8, 293.6, 289.3, 287.4, 286.3, and 285.3 eV, corresponding to the C-$F_3$, C-$F_2$, O-C=C, C=O, C-N, and C–C/C=C groups, respectively [49].

The presence of the C-$F_3$ bond in the LA-CDs-10% was from the Teflon binder used for the LAL processing. The Teflon binder has no effect on the emissions, as shown in Fig. S5 in Supplementary Information. It is evident that both the HTC-CDs and the LA-CDs-10% possessed the C-N groups, which contributed to the PL responses under the UV excitation.

Additional peaks at 1074.3, 687.1, 533.1, 400.8 and 286.4 eV in the XPS spectrum of the LA-CDs-10% are attributed to Na1s, F1s, O1s, N1s and C1s. The presence of the Na1s peak was due to the sodium residual presented in the glassware.

The XPS analyses of the LA-CDs-x% were also performed, as shown in Figs. S2-3 and summarized in Tables S2-3.in Supplementary Information. Similar to LA-CDs-10%, all the other LA-CDs-x% exhibited a strong N1s peak in the range of 400-402 eV, corresponding to the graphitic, pyrrolic, amine and pyridinic nitrogen. All of these results suggest that the LAL processing of the annealed-CDs in $NH_4OH$ solutions is an effective method for doping N to carbon nanoparticles, and the amount of doped-N can be simply controlled by the concentration of the $NH_4OH$ solution.

According to Fig. 4a-b, there exist the PL decay of the HTC-CDs and LA-CDs-10% for 440 and 450 nm emission, respectively, under the 393 nm excitation. By fitting the data to a triple-exponential function, we determined the lifetimes for the corresponding rate processes and the relative contributions, as listed in Table 1.

For the HTC-CDs, the strongest emission is at the wavelength of 440 nm. The lifetime of the intrinsic state ($\tau_1$) at 440 nm emssion was 1.21 ns with the relative contribution of 28.6%. The lifetimes and the relative contributions of the intrinsic state ($\tau_1$) are (1.05 ns, 24.4%) and (1.14 ns, 24.6%) for the emissions with longer wavelengths at 452 and 459 nm, respectively. For the 440 nm emission, the lifetimes and the relative contributions of the surface-functional groups ($\tau_1$ and $\tau_2$) are (4.24 ns, 52.8%) and (15.0 ns, 18.6%), respectively; for the 452 and 459 nm emission, the lifetimes and the relative contributions of the surface-functional groups are [(4.23 ns, 55.0%), (13.6 ns, 20.6%)] and [(4.41 ns, 55.1%), (14.0 ns, 20.3%)], respectively. It is evident that the surface-functional groups played a dominant role in determining the lifetime of the PL responses of the HTC-CDs.

From Table 1, we note that the strongest emission for the LA-CDs-10% is present at 459

nm, and the lifetimes for the intrinsic state and the surface-functional groups are generally less than those for the HTC-CDs under the UV excitation of the same wavelengths. On the other hand, the relativel contributions of the surface functional groups are larger than those for the HTC-CDs. That is to say, there are more contributions from the surface-functional groups in the LA-CDs-10% than those in the HTC-CDs. The LAL processing of the annealed-CDs likely increases the fractions of the surface-functional groups responsible for the PL responses of the soybean-derived CDs.

According to the above discussion, we can conclude that the nitrogen-contained functional groups play the key role in determining the PL responses of the soybean-derived CDs. The LAL processing of the annealed-CDs in $NH_4OH$ solution successfully introduced the surface-functional groups with nitrogen to the CDs, and all the LA-CDs-x% exhibited the PL emission under the UV excitation with a wide range of wavelengths. Under the 390 nm excitation, the wavelengths corresponding to the maximum emission peaks are 464, 459, 463, 462, and 454 nm respectively for the LA-CDs-5%, LA-CDs-10%, LA-CDs-15%, LA-CDs-20% and LA-CDs-30% (Fig. S4). There is no significant difference in the wavelengths corresponding to the maximum emission peaks. However, there exists the dependence of the QY of the PL emission on the fraction/amount of nitrogen.

Figure 9 shows the variations of the atomic fraction of N and QY of the LA-CDs-x% with the concentration of $NH_4OH$. Both the atomic fraction of N and QY of the LA-CDs-x% increase first with the increase of the concentration of $NH_4OH$, reach the maximum, and then decrease with the increase of the concentration of $NH_4OH$. In general, the QY of the LA-CDs-x% is a function of the fraction/amount of nitrogen. There exists a maximum fraction of nitrogen, which can be introduced through the LA-activated surface-functional groups to the Annealed-CDs. Note that the deviation of the QY trend from that of the N atomic fractions at high N contents implies that other factors (i.e., defects) may start to influence the PL responses of the LA-CDs-x% with $x \geq 30\%$.

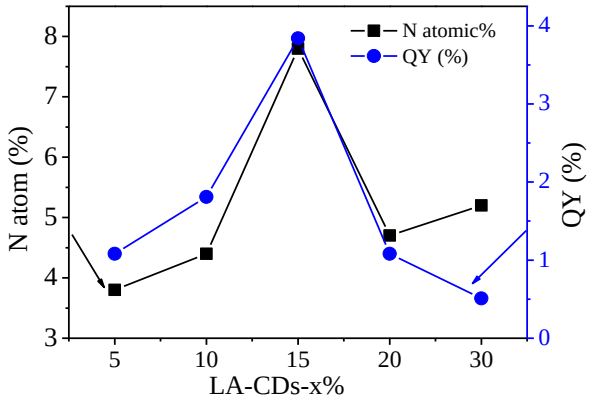


**Figure 9.** Variations of atomic fraction of N and QY of LA-CDs-x% with the concentration of $NH_4OH$

## 5. Summary

In summary, we have synthesized carbon nanoparticles with different PL characteristics from the ground soybean residual via the combination of hydrothermal carbonization, annealing at high temperatures and laser ablation in $NH_4OH$ solution. The annealing of the soybean-derived nanoparticles at high temperatures damaged/destroyed the surface structures of carbon nanoparticles, removed the nitrogen-containing surface functional groups, and resulted in the loss of the PL characteristics. The laser ablation of the annealed soybean-derived nanoparticles in $NH_4OH$ solutions introduced N-contained surface-functional groups, and the atomic fraction of dopped-N by the laser abaltion increased first to a maximum and then decreased with the increase of the concentration of $NH_4OH$. The laser ablation of the annealed soybean-derived nanoparticles reduced the average particle size and narrowed the size distribution.

Both the HTC-CDs and the LA-CDs-x% exihibited the PL characteristics under the UV-Vis excitation due to the presence of N-contained surface-functional groups, even though the PL responses under the UV excitation of the same wavelength were different. The diffifference in the PL responses can be attribued to different amount of the N-contained surface-functional groups, even though both the soybean-derived nanoparticles possessed similar types of the surface groups. The atomic percetanges of nitrogen were 10.3% in the HTC-CDs and 4.4% in the LA-CDs-10%, respectively. The quantum yield of the LA-CDs-x% is a function of the N-fraction for the LA-CDs with up to 30% of N. The QY of the LA-CDs-x% is more stable than

that of the HTC-CDs under continuous UV excitation and showed no significant reduction over the150 min irradiation.

The results presented in this work reveal the important role of the surface-functional groups in controlling the PL responses of CDs and shed insight into the PL mechanisms of the CDs with N-containing surface-functional groups. This work offers a simple, green, and effective strategyfor surface N-functionalization of the carbon nanoparticles derived from biomass and biowaste and for the production of carbon nanoparticlds with stable PL characteristics and excellent water-wettability.

**Acknowledgements**

This work is supported by the NSF through the grant CMMI-1634540 and CMMI-1854554 (FQY) monitored by Dr. Khershed Cooper, the grant CHE-1800316 (DSY) of the Division of Chemistry, and the National Natural Science Foundation of China (No. 21805123) (WS).

**References:**


1. Demchenko, A. P.; Dekaliuk, M. O. Novel Fluorescent Carbonic Nanomaterials for Sensing and Imaging. *Methods Appl. Fluoresc.* **2013**, *1*, 042001.
2. Qu, K.; Wang, J.; Ren, J.; Qu, X. Carbon Dots Prepared by Hydrothermal Treatment of Dopamine as an Effective Fluorescent Sensing Platform for the Label-Free Detection of Iron(III) Ions and Dopamine. *Chem. Eur. J.* **2013**, *19*, 7243–7249.
3. Yang, S.-T.; Wang, X.; Wang, H.; Lu, F.; Luo, P. G.; Cao, L.; Meziani, M. J.; Liu, J.-H.; Liu, Y.; Chen, M.; et al. Carbon Dots as Nontoxic and High-Performance Fluorescence Imaging Agents. *J. Phys. Chem. C* **2009**, *113*, 18110–18114.
4. Wang, W.; Li, Y.; Cheng, L.; Cao, Z.; Liu, W. Water-Soluble and Phosphorus-Containing Carbon Dots with Strong Green Fluorescence for Cell Labeling. *J. Mater. Chem. B* **2014**, *2*, 46–48.
5. Kruss, S.; Hilmer, A. J.; Zhang, J.; Reuel, N. F.; Mu, B.; Strano, M. S. Carbon Nanotubes as Optical Biomedical Sensors. *Adv. Drug Deliv. Rev.* **2013**, *65*, 1933–1950.
6. Sun, Y.-P.; Zhou, B.; Lin, Y.; Wang, W.; Fernando, K. A. S.; Pathak, P.; Meziani, M. J.; Harruff, B. A.; Wang, X.; Wang, H.; et al. Quantum-Sized Carbon Dots for Bright and Colorful Photoluminescence. *J. Am. Chem. Soc.* **2006**, *128*, 7756–7757.
7. Jiang Kai; Sun Shan; Zhang Ling; Lu Yue; Wu Aiguo; Cai Congzhong; Lin Hengwei. Red, Green, and Blue Luminescence by Carbon Dots: Full- Color Emission Tuning and Multicolor Cellular Imaging. *Angew. Chem. Int. Ed.* **2015**, *54*, 5360–5363.
8. Tan, M.; Zhang, L.; Tang, R.; Song, X.; Li, Y.; Wu, H.; Wang, Y.; Lv, G.; Liu, W.; Ma, X. Enhanced Photoluminescence and Characterization of Multicolor Carbon Dots Using Plant Soot as a Carbon Source. *Talanta* **2013**, *115*, 950–956.
9. Sun, X.; He, J.; Meng, Y.; Zhang, L.; Zhang, S.; Ma, X.; Dey, S.; Zhao, J.; Lei, Y. Microwave-Assisted Ultrafast and Facile Synthesis of Fluorescent Carbon Nanoparticles from a Single Precursor: Preparation, Characterization and Their Application for the Highly Selective Detection of Explosive Picric Acid. *J. Mater. Chem. A* **2016**, *4*, 4161–4171.
10. Zhu, C.; Zhai, J.; Dong, S. Bifunctional Fluorescent Carbon Nanodots: Green Synthesis

via Soy Milk and Application as Metal-Free Electrocatalysts for Oxygen Reduction. *Chem. Commun.* **2012**, *48*, 9367–9369.

11. Cui, X.; Wang, Y.; Liu, J.; Yang, Q.; Zhang, B.; Gao, Y.; Wang, Y.; Lu, G. Dual Functional N- and S-Co-Doped Carbon Dots as the Sensor for Temperature and Fe3+ Ions. *Sens. Actuators B* **2017**, *242*, 1272–1280.
12. Chen, X.; Kis, A.; Zettl, A.; Bertozzi, C. R. A Cell Nanoinjector Based on Carbon Nanotubes. *Proc. Natl. Acad. Sci.* **2007**, *104*, 8218–8222.
13. Cao, L.; Yang, S.-T.; Wang, X.; Luo, P. G.; Liu, J.-H.; Sahu, S.; Liu, Y.; Sun, Y.-P. Competitive Performance of Carbon "Quantum" Dots in Optical Bioimaging. *Theranostics* **2012**, *2*, 295–301.
14. Qiao, Z.-A.; Wang, Y.; Gao, Y.; Li, H.; Dai, T.; Liu, Y.; Huo, Q. Commercially Activated Carbon as the Source for Producing Multicolor Photoluminescent Carbon Dots by Chemical Oxidation. *Chem. Commun.* **2010**, *46*, 8812–8814.
15. Chen, G. X.; Hong, M. H.; Chong, T. C.; Elim, H. I.; Ma, G. H.; Ji, W. Preparation of Carbon Nanoparticles with Strong Optical Limiting Properties by Laser Ablation in Water. *J. Appl. Phys.* **2004**, *95*, 1455–1459.
16. Lai, C.-W.; Hsiao, Y.-H.; Peng, Y.-K.; Chou, P.-T. Facile Synthesis of Highly Emissive Carbon Dots from Pyrolysis of Glycerol; Gram Scale Production of Carbon Dots/MSiO 2 for Cell Imaging and Drug Release. *J. Mater. Chem.* **2012**, *22*, 14403–14409.
17. Wang, C.; Xu, Z.; Cheng, H.; Lin, H.; Humphrey, M. G.; Zhang, C. A Hydrothermal Route to Water-Stable Luminescent Carbon Dots as Nanosensors for pH and Temperature. *Carbon* **2015**, *82*, 87–95.
18. Sevilla, M.; Fuertes, A. B. Chemical and Structural Properties of Carbonaceous Products Obtained by Hydrothermal Carbonization of Saccharides. *Chem. Eur. J.* **2009**, *15*, 4195–4203.
19. Yang, Y.; Cui, J.; Zheng, M.; Hu, C.; Tan, S.; Xiao, Y.; Yang, Q.; Liu, Y. One-Step Synthesis of Amino-Functionalized Fluorescent Carbon Nanoparticles by Hydrothermal Carbonization of Chitosan. *Chem. Commun.* **2012**, *48*, 380–382.
20. Sahu, S.; Behera, B.; K. Maiti, T.; Mohapatra, S. Simple One-Step Synthesis of Highly

Luminescent Carbon Dots from Orange Juice: Application as Excellent Bio-Imaging Agents. *Chem. Commun.* **2012**, *48*, 8835–8837.

21. Liu, S.; Tian, J.; Wang, L.; Zhang, Y.; Qin, X.; Luo, Y.; Asiri, A. M.; Al- Youbi, A. O.; Sun, X. Hydrothermal Treatment of Grass: A Low-Cost, Green Route to Nitrogen-Doped, Carbon-Rich, Photoluminescent Polymer Nanodots as an Effective Fluorescent Sensing Platform for Label-Free Detection of Cu(II) Ions. *Adv. Mater.* **2012**, *24*, 2037–2041.
22. Zeng, H.; Du, X.-W.; Singh, S. C.; Kulinich, S. A.; Yang, S.; He, J.; Cai, W. Nanomaterials via Laser Ablation/Irradiation in Liquid: A Review. *Adv. Funct. Mater.* **2012**, *22*, 1333–1353.
23. Liu, P.; Cui, H.; Wang, C. X.; Yang, G. W. From Nanocrystal Synthesis to Functional Nanostructure Fabrication: Laser Ablation in Liquid. *Phys. Chem. Chem. Phys.* **2010**, *12*, 3942–3952.
24. Amendola, V.; Meneghetti, M. What Controls the Composition and the Structure of Nanomaterials Generated by Laser Ablation in Liquid Solution? *Phys. Chem. Chem. Phys.* **2013**, *15*, 3027–3046.
25. Yang, L.; May, P. W.; Yin, L.; Smith, J. A.; Rosser, K. N. Growth of Diamond Nanocrystals by Pulsed Laser Ablation of Graphite in Liquid. *Diam. Relat. Mater.* **2007**, *16*, 725–729.
26. Li, Z. F.; Yang, Z. Y.; Xiao, R. F. Visible Photoluminescence from Hydrogenated Amorphous Carbon Films Prepared by Pulsed Laser Ablation of Polymethyl Methacrylate (PMMA). *Appl. Phys. A* **1996**, *63*, 243–246.
27. Baker, S. N.; Baker, G. A. Luminescent Carbon Nanodots: Emergent Nanolights. *Angew. Chem. Int. Ed.* **2010**, *49*, 6726–6744.
28. Zhu, S.; Song, Y.; Zhao, X.; Shao, J.; Zhang, J.; Yang, B. The Photoluminescence Mechanism in Carbon Dots (Graphene Quantum Dots, Carbon Nanodots, and Polymer Dots): Current State and Future Perspective. *Nano Res.* **2015**, *8*, 355–381.
29. Xu, Y.; Wu, M.; Liu, Y.; Feng, X.-Z.; Yin, X.-B.; He, X.-W.; Zhang, Y.-K. Nitrogen-Doped Carbon Dots: A Facile and General Preparation Method, Photoluminescence Investigation, and Imaging Applications. *Chem. Eur. J. 19*, 2276–2283.

30. Bartlett, J. S.; Voss, K. J.; Sathyendranath, S.; Vodacek, A. Raman Scattering by Pure Water and Seawater. *Appl. Opt.* **1998**, *37*, 3324–3332.
31. Jia, X.; Li, J.; Wang, E. One-Pot Green Synthesis of Optically PH-Sensitive Carbon Dots with Upconversion Luminescence. *Nanoscale* **2012**, *4*, 5572–5575.
32. Wu, Q.; Li, W.; Tan, J.; Wu, Y.; Liu, S. Hydrothermal Carbonization of Carboxymethylcellulose: One-Pot Preparation of Conductive Carbon Microspheres and Water-Soluble Fluorescent Carbon Nanodots. *Chem. Eng. J.* **2015**, *266*, 112–120.
33. Calabro, R. L.; Yang, D.-S.; Kim, D. Y. Liquid-Phase Laser Ablation Synthesis of Graphene Quantum Dots from Carbon Nano-Onions: Comparison with Chemical Oxidation. *J. Colloid Interface Sci.* **2018**, *527*, 132–140.
34. Liu, Y.; Young Kim, D. Ultraviolet and Blue Emitting Graphene Quantum Dots Synthesized from Carbon Nano-Onions and Their Comparison for Metal Ion Sensing. *Chem. Commun.* **2015**, *51*, 4176–4179.
35. Wang, H.; Sun, P.; Cong, S.; Wu, J.; Gao, L.; Wang, Y.; Dai, X.; Yi, Q.; Zou, G. Nitrogen-Doped Carbon Dots for "Green" Quantum Dot Solar Cells. *Nanoscale Res. Lett.* **2016**, *11*, 27.
36. Wang, L.; Zhu, S.; Wang, H.; Qu, S.; Zhang, Y.; Zhang, J.; Chen, Q.; Xu, H.; Han, W.; Yang, B.; Sun, H. Common Origin of Green Luminescence in Carbon Nanodots and Graphene Quantum Dots, *ACS Nano* **2014**, *8*, 2541–2547.
37. Li, X.; Wang, H.; Shimizu, Y.; Pyatenko, A.; Kawaguchi, K.; Koshizaki, N. Preparation of Carbon Quantum Dots with Tunable Photoluminescence by Rapid Laser Passivation in Ordinary Organic Solvents. *Chem. Commun.* **2011**, *47*, 932–934.
38. Yu, P.; Wen, X.; Toh, Y.-R.; Tang, J. Temperature-Dependent Fluorescence in Carbon Dots. *J. Phys. Chem. C* **2012**, *116*, 25552–25557.
39. Stuart, B. Infrared Spectroscopy. In *Kirk-Othmer Encyclopedia of Chemical Technology*; American Cancer Society, 2015; pp 1–18.
40. Socrates, G. *Infrared and Raman Characteristic Group Frequencies: Tables and Charts*; John Wiley & Sons, 2004.
41. Lieber, E.; Levering, D. R.; Patterson, L. Infrared Absorption Spectra of Compounds of

High Nitrogen Content. *Anal. Chem.* **1951**, *23*, 1594–1604.

42. Camacho, N. P.; West, P.; Torzilli, P. A.; Mendelsohn, R. FTIR Microscopic Imaging of Collagen and Proteoglycan in Bovine Cartilage. *Biopolymers* **2001**, *62*, 1–8.
43. Pavia, D. L.; Lampman, G. M.; Kriz, G. S.; Vyvyan, J. A. *Introduction to Spectroscopy*; Cengage Learning, 2008.
44. Hirschfeld, T.; Chase, B. FT-Raman Spectroscopy: Development and Justification. *Appl. Spectrosc.* **1986**, *40*, 133–137.
45. Mohtasebi, A.; Chowdhury, T.; Hsu, L. H. H.; Biesinger, M. C.; Kruse, P. Interfacial Charge Transfer between Phenyl-Capped Aniline Tetramer Films and Iron Oxide Surfaces. *J. Phys. Chem. C* **2016**, *120*, 29248–29263.
46. Wahid, M.; Parte, G.; Phase, D.; Ogale, S. Yogurt: A Novel Precursor for Heavily Nitrogen Doped Supercapacitor Carbon. *J. Mater. Chem. A* **2014**, *3*, 1208–1215.
47. Li, X.; Zhang, S.; Kulinich, S. A.; Liu, Y.; Zeng, H. Engineering Surface States of Carbon Dots to Achieve Controllable Luminescence for Solid-Luminescent Composites and Sensitive $Be^{2+}$ Detection. *Sci. Rep.* **2014**, *4*, 4976.
48. Lu, S.; Cong, R.; Zhu, S.; Zhao, X.; Liu, J.; S.Tse, J.; Meng, S.; Yang, B. PH-Dependent Synthesis of Novel Structure-Controllable Polymer-Carbon NanoDots with High Acidophilic Luminescence and Super Carbon Dots Assembly for White Light-Emitting Diodes. *ACS Appl. Mater. Interfaces* **2016**, *8*, 4062–4068.
49. Yang, Z.; Xu, M.; Liu, Y.; He, F.; Gao, F.; Su, Y.; Wei, H.; Zhang, Y. Nitrogen-Doped, Carbon-Rich, Highly Photoluminescent Carbon Dots from Ammonium Citrate. *Nanoscale* **2014**, *6*, 1890–1895.